The role of ionomers in the electrolyte management of zero-gap MEA-based CO$_2$ electrolysers: A Fumion *vs.* Nafion comparison

Menglong Liu [a], Huifang Hu [a], Ying Kong [a], Iván Zelocualtecatl Montiel [a], Viliam Kolivoška [b], Alexander V. Rudnev [a,c], Yuhui Hou [a], Rolf Erni [d], Soma Vesztergom [a,e,*], Peter Broekmann [a,**]

[a] *NCCR Catalysis, University of Bern, Department of Chemistry, Biochemistry and Pharmaceutical Sciences, Freiestrasse 3, 3012 Bern, Switzerland*
[b] *J. Heyrovský Institute of Physical Chemistry of the Czech Academy of Sciences, Dolejškova 3, 182 23 Prague, Czechia*
[c] *A. N. Frumkin Institute of Physical Chemistry and Electrochemistry, Russian Academy of Sciences, Leninsky Prospekt 31, 119071 Moscow, Russia*
[d] *Electron Microscopy Center, Swiss Federal Laboratories for Materials Science and Technology (EMPA), Überlandstrasse 129, 8600 Dübendorf, Switzerland*
[e] *Eötvös Loránd University, MTA–ELTE Momentum Interfacial Electrochemistry Research Group, Pázmány Péter sétány 1/A, 1117 Budapest, Hungary*

ARTICLE INFO

ABSTRACT

We study the role of binders (ionomers) in determining the life-span of gas diffusion electrodes (GDEs) used for high throughput CO$_2$-to-CO electrolysis. We compare two typical ionomer materials (Nafion and Fumion, both are widely used for the preparation of Ag nanoparticles-based catalyst inks) to show that when used in zero-gap membrane/electrode assemblies, Fumion-containing inks are superior to Nafion-based ones and can uphold a very high CO-selectivity in the electrochemical CO$_2$ reduction reaction for longer time. This is due to the ability of Fumion containing inks to suppress precipitation inside the GDE structure. As Fumion-fixed GDEs are significantly less hydrophobic than Nafion-fixed ones, our results contradict the widely accepted opinion that it is their non-wettability what mostly protects CO$_2$-reducing GDEs from flooding. In turn, we argue that it is more important to maintain efficient electrolyte drainage pathways in the GDE structure, and explain the superiority of Fumion-fixed GDEs on this basis.

1. Introduction

The increasing level of atmospheric carbon dioxide (CO$_2$) and its climatic and environmental consequences, such as global warming and ocean acidification, present a serious threat to the sustainable development of human society [1]. Propelled by the excess of intermittent energy sources, the electrochemical CO$_2$ reduction reaction (*ec*–CO$_2$RR) is a promising approach to convert CO$_2$ into valuable fuels and commodity chemicals [1–3], and thereby to restore the global carbon cycle.

Depending on the catalyst applied for the reaction, *ec*–CO$_2$RR can yield a variety of products that even include hydrocarbons [4] and alcohols [5,6] of various (typically 1–3 carbon atoms) chain lengths [7,8]. However, from an economic point of view, those that lead to the formation of carbon monoxide (CO) and formate (HCOO$^-$) are considered the most viable amongst the various possible reaction routes. This is mostly because the two-electron transfer that leads to CO and formate production offers a large profit margin over other multi-electron transfer

products that require heavier energy inputs [9]. Strong cases of commercial viability can be made especially for the production of CO, as CO is considered a remarkably versatile precursor of the production of synthetic fuels [9], and industrial applications already exist for the coupling of CO$_2$ and water co-electrolysers to fermentation modules where CO and H$_2$ are converted to butanol and hexanol with high carbon selectivity [10]. Amongst the various metal catalysts (Au, Ag, Zn, Pd, Ga) that direct *ec*–CO$_2$RR towards the formation of CO [11], Ag-based ones seem to be the most promising [12–14].

By using Ag especially in the form of nanoparticles (NPs) for the catalysis of *ec*–CO$_2$RR, Faradaic efficiencies (*FE*s) reaching almost 100% in the CO$_2$-to-CO conversion can be achieved [12], and at least in standard lab-scale experiments utilising conventional "H-type" cells, the reaction can remain stable for a very long time. The up-scaling of the reaction in the direction of reaching industrially relevant reaction rates is still hindered, however, by several tough challenges, and addressing these requires not only the study of new catalyst materials, but also that

of entire electrolyser designs [16,17].

In a conventional H-type cell, where CO_2 dissolved in an aqueous phase undergoes reduction at the electrode surface, the reaction quickly becomes mass transport limited at high enough cathodic potentials, and the reaction rate will thus not be determined by the catalytic activity of the cathode but rather by the slow diffusion and low concentration of water-dissolved CO_2 molecules, allowing current densities typically not exceeding a few mA cm^{-2} in quiescent solutions. To overcome this limitation, and to achieve current densities that are orders of magnitude higher, the application of gas diffusion electrodes (GDEs) seems to be intuitive [18–28].

In GDEs, the catalyst is supported by a gas diffusion layer (GDL) that is composed of a carbon fibrous layer (CFL) and a microporous layer (MPL), as shown in Fig. 1a, and this bi-layer structure allows CO_2 to reach the catalyst layer essentially in gas phase, relieving the mass transport limitations that apply to H-type cells. Besides enabling fast reactant delivery, the GDL also facilitates the release of gaseous reaction products, serves as a mechanical support and electrical contact for the catalyst, and plays important role in controlling the amount of electrolyte in the catalyst layer [29].

In practical electrolysers producing mostly gaseous products, GDEs are often applied as parts of so-called zero-gap membrane-electrode assemblies (MEAs, Fig. 1), where the GDE is directly interfaced to an anion exchange membrane [30,31]. The membrane [32] assures that no volatile cathode-generated products cross over to the anode, which would reduce the efficiency of electrolysis. Another important role of the anion exchange membrane in zero-gap MEAs is that it controls the access of water to the catalyst layer while making sure that anionic reaction byproducts and products of CO_2 neutralisation —e.g., hydroxide and (bi-)carbonate ions— can be transported away from it.

Water plays a very ambiguous role in MEA-based CO_2-to-CO electrolysers [23,33]. Since water appears as a reactant in the target reaction

$$CO_2 + H_2O + 2e^- \rightarrow CO + 2OH^-, \tag{R1}$$

the presence of some amount of water in or nearby the catalyst layer is essential. If, however, an excess amount of water penetrates not only the catalyst layer but the underlying MPL as well, it may flood micropores, thereby blocking the access of CO_2 to the catalyst and giving rise to parasitic hydrogen evolution:

$$2H_2O + 2e^- \rightarrow H_2 + 2OH^-. \tag{R2}$$

As of today, it is probably the above-mentioned proneness of GDE micropores to flooding that presents the main obstacle in front of the scale-up prospects of CO_2 electroreduction [21,34–39]. When flooding in a GDE-based electrolyser occurs to such extent that the reactant CO_2 can no longer reach the catalyst layer, severe stability issues —a shifting from Reaction (R1) to (R2)— occur, and as a result, the *FE* of CO formation drops down during long-time electrolyses.

In zero-gap MEAs, the penetration of water (or in fact, that of the KOH solution) through the membrane cannot be precisely controlled, and usually the amount of electrolyte passing through the membrane is more than what could be consumed by Reaction (R1). In order to avoid that this excess amount of electrolyte gets trapped within (and ultimately floods) the micropores of the GDL, measures have to be taken to allow its drainage through the microporous and then the carbon fibrous layer, so that it can eventually exit the electrolyser with the outward gas flow. As it was pointed out recently [15,40–42], maintaining the efficacy of drainage channels by which the above-described perspiration [43,44] occurs seems to be a key strategic line in avoiding the flooding of MPL micropores, and thus extending the lifetime of zero-gap MEA-based CO_2 electrolysers.

The task of optimising electrolyte management in zero-gap MEAs is further complicated by the fact that most of these constructions apply heavily alkaline electrolyte solutions (to keep the anode process fast enough) and by that the anion exchange membranes used for the separation of the cathode GDE from the anode compartment are to some extent permeable also to cations.

When cations of the anolyte (in our case, K^+ ions) appear on the cathode GDE, they react with the CO_2 supply and form K_2CO_3/$KHCO_3$ salts. If these salts are formed only in a small amount, they present less of a threat as they can perspire through the GDL and exit the electrolyser dissolved in aerosol. If, on the other hand, K_2CO_3/$KHCO_3$ salts are formed at large concentrations, they precipitate inside the GDE structure or over the catalyst layer, which can have a detrimental effect on the electrolysis process [43,45]. Following electrolysis, K_2CO_3/$KHCO_3$ precipitates can often be visualised, e.g., by energy dispersive X-ray (EDX)-based analysis, inside or on top of the GDE structure [41].

The EDX elemental mapping-based analysis of precipitate formation patterns in GDEs, combined with the inductively coupled plasma mass
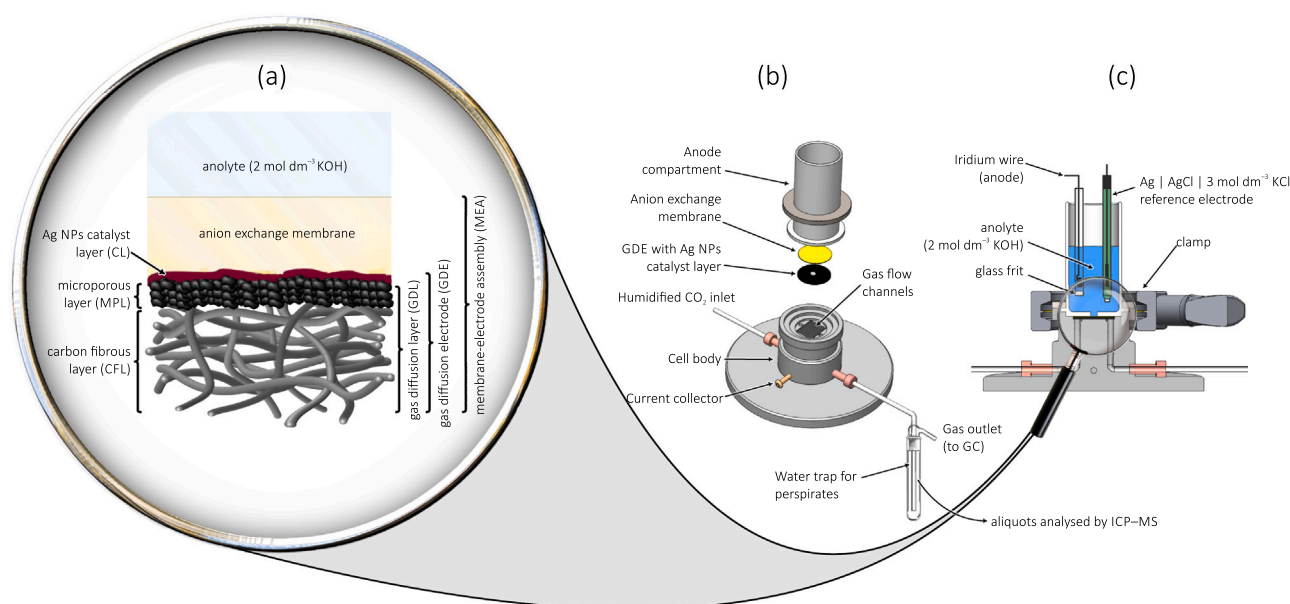

Fig. 1. A zero-gap membrane-electrode assembly (MEA) employing a gas diffusion electrode in contact with an anion exchange membrane, used in a gas-flow cell for the electrolysis of CO_2. Part (a) shows a close-up view of the MEA, parts (b) and (c) show the exploded and the cross-sectional view of the electrolyser. Adapted from [15].

spectrometry (ICP–MS) -based monitoring of K^+ outflow can lead to a better understanding of the often-observed stability losses of zero-gap MEA-based CO_2 electrolysers [41], and the combination of these methods have already led to the successful identification of design strategies that could help prolong electrolyser lifespans. These strategies included the preferential application of GDLs with a cracked MPL structure (over GDLs of compact MPLs, [42]) or the practice of avoiding the use of polymeric capping agents when formulating Ag NP-based catalyst inks [15].

In the present paper we focus on another important constituent of zero-gap MEAs that has crucial effect on the water (electrolyte) management of electrolysers. This constituent is the binder: an ionomer that is added to the catalyst ink in order to improve its consistency, its electrical (ionic) conductivity, and its adherence to the MPL surface. In this paper we compare two well-known binders, Nafion and Fumion, in order to study their effect on the lifespan of electrolyses.

The major difference between the two applied binders is that Nafion, a sulphonated tetrafluoroethylene-based polymer, is an essentially H^+-conducting material, while Fumion, a polyaromatic polymer with quaternary ammonium functional groups, conducts electricity by counterion (in the studied media, OH^- or CO_3^{2-}/HCO_3^-) hopping. While, probably mostly out of tradition, Nafion is still used by a vast majority of researchers of *ec*–CO_2RR as the ionomer of cathode catalyst layers (see [46] for a Review), the advantages of using anion exchange ionomers (especially in order to hinder cation penetration and precipitation at the cathode) were also identified [47].

Working under the hypothesis that upholding effective perspiration is essential in order to avoid the entrapment of electrolyte (flooding) in the GDE structure, as well as that the appearance of K^+ ions inside the GDE can directly be interpreted as a tracer of flooding, we utilise our recently developed approach [31] that combines post-experimental EDX-based analysis of GDEs with the ICP–MS-based monitoring of perspired electrolytes in order to shed light on the reasons why the application of Fumion as a binder leads to more prolonged electrolysis stability compared to when a Nafion ionomer is used for the fixation of the catalyst ink.

We note here that a recent comparative study by Nwabara et al. on different ionomers [48], the scope of which also initially included Fumion, concluded —based on contact angle measurements screening— that Fumion would not be an efficient binder because of its hydrophobicity being significantly lower than that of Nafion. While this observation is generally valid (and in contact angle measurements we also observed the same difference), this paper points out that the ability of ionomers to assure effective electrolyte perspiration, thus enabling longer electrolysis stability, is a more important factor than hydrophobicity alone. This observation, we believe, is an important addition to existing screening strategies that seem to emphasise mostly the role of non-wettability in GDE design for stable *ec*–CO_2RR [48–51].

With regard to the zero-gap cathode MEA configuration used in our experiments (see Fig. 1) we note here that this set-up was created specifically for the accelerated durability testing of CO_2 electrolysing GDEs [22]. As opposed to devices of higher effective surface areas employing a true zero-gap configuration that also includes an anode GDE, the effective area of our small-scale electrolyser is only a few square-millimetres, and it features a semi-zero gap design, meaning that the membrane is brought into direct contact with the anolyte solution containing an Ir wire anode and is not interfaced to an anode GDE. As a result of these two conceptual differences, stability defects in our small-scale electrolyser can be observed after much shorter times of electrolysis, compared to semi-industrial scale reactors where durability issues similar to those reported in our paper would occur only after weeks of stable operation [52].

2. Experimental

2.1. Chemicals used

All chemicals were used as purchased, without further purification. Potassium hydroxide (reagent grade, 90%, flakes) and Nafion (Nafion 117, $w \approx 5\%$, dissolved in a mixture of lower aliphatic alcohols and water) were purchased from Sigma-Aldrich. Dispersions of lipoic acid capped —for some experiments, polyvinylpyrrolidone (PVP) capped or branched polyethylene-imine (BPEI) capped— Ag NPs (1 mg cm^{-3} Ag in 2 mmol dm^{-3} aqueous K_2CO_3 solution) were purchased from Nano-Composix. The Freudenberg H23C8 GDL and Fumion solution (Fumion FAA-3-SOLUT-10) were purchased from Fuel Cell Store. Carbon black (Vulcan XC 72 R) was purchased from Cabot. Isopropanol (VLSI Selectipur) was obtained from BASF. The anion exchange membrane (X3750 RT) was purchased from Dioxide materials. Ir wire (99.9%) was obtained from MaTeck Material Technologie & Kristalle GmbH. An Ag | AgCl | 3 mol dm^{-3} KCl reference electrode (double junction design) was purchased from Metrohm. Carbon dioxide (99.999%) was purchased from Carbagas. Ultra-pure water (Milli-Q by Merck Millipore, 18.2 MΩ cm specific resistance) was used in all experiments.

2.2. Catalyst ink preparation

0.25 cm^3 of the dispersion containing lipoic acid (alternatively, for some experiments, PVP or BPEI) capped Ag NPs and 0.74 cm^3 of carbon black in isopropanol (carbon concentration: 0.059 mg cm^{-3}) were separately sonicated for 10 min. Then, the two solutions were mixed, and 0.01 cm^3 of either Nafion or Fumion binder solutions (as purchased) was added, following which the resulting ink was sonicated for another 10 min. We note here that if no binder is used, the ink becomes unstable and already within 10 min, agglomeration of particles can be observed (see the photos of Fig. S1 in Supporting Information). The amount of binders to add (0.01 cm^3 in 1 cm^3 ink, corresponding to 1% binder volume fraction) was determined based on pre-screening experiments, results of which are shown in Fig. S2 of Supporting Information. In case when the Fumion binder was used, the ink of 1% binder volume fraction exhibited the longest durability during electrolyses. In case of Nafion, the binder concentration had little effect on the stability of electrolysis, thus we decided to compare inks with the same, 1% binder volume fraction. As seen in Fig. S1, these catalyst inks were homogeneous, with an Ag NP concentration of 0.25 mg cm^{-3} and an Ag/carbon black mass ratio of 85:15.

2.3. Preparation of the GDEs

0.04 cm^3 of the prepared catalyst ink was drop-cast on the centre of the microporous surface of a circular Freudenberg H23C8 (FuelCell-Store) GDL of 2 cm diameter by using vacuum filtration. By applying a silicone plate mask, the drop-cast area was limited to a circle of 4 mm diameter. The thus prepared GDE was dried in a vacuum drying chamber overnight.

2.4. Assembly of the electrolyser

The electrolyser shown in Fig. 1 was used to carry out electrochemical CO_2 reduction. The bottom part of the electrolyser is made of stainless steel and is equipped with gas flow channels, on which the prepared GDEs were placed with the catalyst layer facing upwards and the bottom carbon fibre layer facing the gas flow channels. The GDE was covered by a hydroxide functionalised Sustainion anion exchange membrane from above, before fixing the Teflon-made anode compartment on top. The anode compartment has a central orifice on its bottom, allowing access of the anolyte to the membrane. The orifice is of 3 mm diameter, determining the geometric surface area (0.0707 cm^2) of the GDE. The anode compartment is filled with 10 cm^3 of 2 mol dm^{-3} KOH

solution, and contains an Ag | AgCl | 3 mol dm^{-3} KCl reference electrode and an Ir wire anode. The anode is placed inside a small chamber and is separated from the rest of the anolyte by glass frit, as shown in Fig. 1.

2.5. Electrochemical measurements and product analysis

All galvanostatic electrolysis experiments were carried out using an ECi-200 potentiostat (Nordic Electrochemistry), by applying a current of -21.2 mA (corresponding to a geometric surface area-normalised current density of -300 mA cm^{-2}) for a duration of 1 h, resulting in a passage of -76.34 C of charge (-1080 C cm^{-2} normalised to geometric surface area). Cathode potentials reported in the paper are all referred to the applied Ag | AgCl | 3 mol dm^{-3} KCl reference electrode. Potential values were IR-corrected based on an impedimetric determination of the series cell resistance. Gaseous reaction products (CO and H$_2$) were analysed by connecting the gas outlet of the electrolyser to a gas chromatograph (GC, SRI Instruments Multigas Analyzer). The continuous flow of the carrier CO$_2$ gas through the cathode flow channels carried reaction products from the gas outlet of the electrolyser into the sampling loop of the gas chromatograph. The partial current I_i, corresponding to the formation of a gaseous product i, can be calculated [53] as

$$I_i = x_i \, n_i \, F \, v_\mathrm{m}, \tag{1}$$

where x_i denotes the mole fraction of the products, determined by GC using an independent calibration standard gas (Carbagas); n_i is the number of electrons involved in the reduction reaction to form a particular product ($n = 2$ for both CO and H$_2$ formation); $F = 96,485.3$ C mol^{-1} is Faraday's constant; and v_m is the molar CO$_2$ gas flow rate determined by a universal flowmeter (7000 GC flowmeter, Ellutia) at the gas outlet of the electrolyser. The Faradaic efficiency (*FE*) of a given reaction product was determined by dividing the respective partial current, calculated from Eq. (1), by the total current. A thermal conductivity detector (TCD, for the detection of H$_2$) and a flame ionisation detector (FID, for the detection of CO) were equipped to the gas chromatograph. In all our experiments, the formed CO and H$_2$ amounts accounted for an altogether 90–99% *FE*. Following 1-hour electrolyses, some amounts of formate (HCOO$^-$) were detected in the anolyte compartment, which could account for the less than 100% total *FE*, although an exact quantification of this product is not possible (due to the fact that it is partially consumed by oxidation at the anode).

2.6. Scanning electron microscope (SEM), energy-dispersive X-ray spectroscopy (EDX) and transmission electron spectroscopy (TEM)

A Zeiss Gemini 450 scanning electron microscope with InLens secondary electron detector and backscattering detector was used to study the surface and the interior of GDEs prior to, and after electrolysis. An accelerating voltage of 5 kV and a beam current of 120 pA were applied at working distances between 5.0 and 5.5 mm. The SmileView software was used to measure the particle size of Ag NPs, 500–700 particles were analyzed at each experimental setting to create particles size distribution charts. To study the morphological evolution of Ag NPs upon electrolysis, all GDEs were immersed into Milli-Q water at least 15 min for three times, to remove K$_2$CO$_3$/KHCO$_3$ precipitates from their surface. (This step was obviously omitted before the SEM/EDX-based characterisation of the formed precipitate patterns.) An Energy Dispersive X-Ray Analyzer (EDX) was used to provide elemental identification and compositional information of Ag and K for after-electrolysis GDE samples. To obtain surface or cross-sectional mapping of GDEs, the Aztec 5.0 software (Oxford Instruments) was used, with an acceleration voltage of 10 kV, current of 1 nA and working distance of 8.5 mm. Cross-sectional SEM and EDX analysis was carried out using the GDE cut by a knife in the middle, by applying pressure to the knife from the back side. For the transmission electron microscopy (TEM) imaging, an FEI Titan Themis

instrument was used with an accelerating voltage of 300 kV.

2.7. Inductively coupled plasma mass spectrometry (ICP–MS)

ICP–MS (NExION 2000, Perkin Elmer) was applied to determine the mass of potassium that perspired through the membrane and the GDE, and exited the electrolyser through the gas outlet. A trap containing 10 cm^3 of ultrapure water was used to collect perspired potassium salts (Fig. 1b). 0.02 cm^3 aliquots of the trap content, collected every 10 min, were 500-fold diluted by an appropriate amount of 2% HNO$_3$ solution (BASF SE, Ludwigshafen, Germany) and the resulting solution samples were injected into the ICP–MS to obtain the content of potassium in perspiration. To determine the Ag mass loading of the GDE samples, the GDEs were immersed in 1 cm^3 of concentrated HNO$_3$ (69.3%, BASF SE, Ludwigshafen, Germany) for 24 h to dissolve all Ag NPs. 0.02 cm^3 of the resulting solutions was diluted with 3% HNO$_3$ solution by a factor of 500, and was then fed into the ICP–MS. Loading values reported in the paper are 95% confidence intervals, calculated from 6 independent measurements.

2.8. Contact angle measurements

Contact angle measurements were carried out using a Krüss Advance Drop Shape Analyzer DSA25 (Krüss GmbH, Hamburg, Germany). GDEs were mounted on a flat stage and water drops (milli-Q water, 0.0014 cm^3) were deposited at room temperature.

Raw data, as well as unprocessed measurement files serving as a basis of this publication can be downloaded from Zenodo [54].

3. Results and discussion

The aim of this paper is to study the effect of two chosen ionomers (Nafion and Fumion) on the stability of *ec*–CO$_2$RR carried out in the electrolyser shown in Fig. 1. This reactor is a small-scale version of catholyte-free (also known as zero-gap) gas fed MEA-based electrolysers [45] in which cathode GDEs are directly interfaced to an anion exchange membrane. Although its small active GDE area (0.0707 cm^2, see the Experimental section for details) limits the operating current of the device (so that it definitely falls short of industrial requirements), the electrolyser can be operated at high ($>$ 100 mA cm^{-2}) current densities. Since it was designed [30,31], the device has become a useful tool for the simulation of close-to application electrolysis conditions, and —complemented by the quantitative monitoring of perspired electrolyte amounts and by the post-mortem SEM/EDX-based analysis of GDEs— the small-scale electrolyser has already successfully been used to identify the major causes of efficiency losses [15,40–42] in GDE-based CO$_2$-to-CO converters.

Due to its limited size, our small-scale electrolyser device is more sensitive to edge effect-related stability losses, thus when operated at suitably high current densities, a break-down of the electrolysis efficiency can be observed relatively early (usually, within an hour). This allows the identification of major malfunction causes without the need of long-lasting electrolyses, and the device can thus serve for the accelerated durability testing of GDEs, the need of which has been pointed out recently [22].

3.1. Characterisation of as-prepared GDEs

Nafion- and Fumion-fixed GDEs were prepared as described in the Experimental Section by keeping the following two points in mind: First, we intentionally applied a Freudenberg H23C8 GDL, the MPL of which is free of any cracks or voids, the size of which would exceed the submicron region. This choice was necessary in order to make sure that we study a "worst-case scenario", in which larger cracks can provide no drainage channels in addition to those provided by micropores [42]. Second, we chose an Ag NP dispersion for the formulation of the catalyst

ink in which the NPs were capped by lipoic acid, a non-polymeric agent that stabilises the NPs mostly by Coulomb interactions, and that does not get adhered to the MPL, clogging its micropores [15].

Although the applied silver loading was almost the same in case of the Nafion-fixed ((37.7 ± 6.0) μg cm^{-2}) and the Fumion-fixed ((40.0 ± 6.5) μg cm^{-2}) GDE, sessile water drop tensiometry (respective contact angles: $150.9° \pm 0.1°$ and $99.8° \pm 0.5°$) revealed that the surface of the Fumion-bound catalyst layer is significantly less hydrophobic, in agreement with previous reports of Nwabara et al. [48].

While TEM investigations (see Fig. S3 of Supporting Information) reveal that Ag NPs originating from Nafion- and Fumion-containing samples have a rather similar nanoscale structure, the SEM/EDX-based imaging of as-prepared GDEs exhibit significant differences. The top-down SEM micrographs (Fig. 2) of the Fumion-bound catalyst layer were relatively blurry, and they showed an apparently smaller number of Ag NPs compared to the much sharper micrographs taken from the Nafion-bound catalyst layer where not only the Ag NPs, but also flakes of the Vulcan carbon support could well be identified. We ascribe the observed blurriness of the SEM images taken from the Fumion-bound catalyst to the formation of an electron-optically dense, jelly-like Fumion layer that covers most of the Ag NPs, keeping them partially inaccessible to the electron beam. This argument is further supported by the cross-sectional SEM micrographs and elemental (Ag) EDX maps of the GDEs. These show that while the Ag NPs of Nafion-bound catalyst inks can relatively deeply penetrate the MPL (to an approximate depth of ~10 μm), such penetration does not occur in Fumion-fixed GDEs. In the latter case it seems that Fumion, probably due to its hydrophilic nature, cannot enter the (hydrophobic) MPL, and as a result, the catalyst forms a well-discernible (about 500 nm thick) layer on top of the GDE.

3.2. Electrolysis stress tests: stability–perspiration relations

Nafion-fixed and Fumion-fixed GDEs also exhibit several differences when made subject to 1 h ec–CO$_2$RR stressing experiments at a high current density (–300 mA cm^{-2}, Fig. 3). Fig. 3a shows that at the start of electrolysis, both GDEs perform well and yield CO with a Faradaic efficiency of $FE_{CO} \geq 90\%$. The performance of the GDEs will then decrease, however, and a shift from CO$_2$-to-CO reduction (Reaction (R1)) to hydrogen evolution (Reaction (R2)) is clearly indicated both by
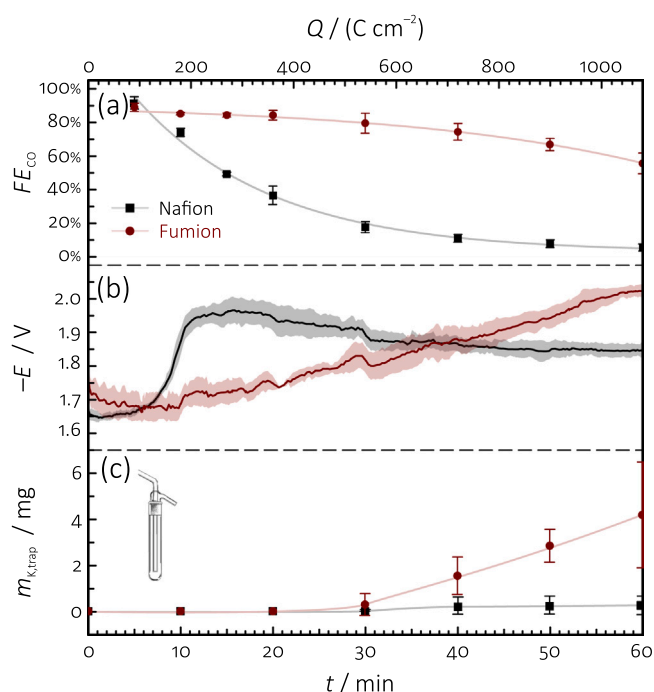
Fig. 3. Results of ec–CO$_2$RR stressing of Nafion-fixed (black) and Fumion-fixed (red) GDEs. Panel (a) shows the variation of the Faradaic efficiency of CO, FE_{CO}, over time. Panel (b) shows the temporal variation of the measured electrode potential E, while in panel (c) we plotted the amount of K$^+$ that perspired through the electrolyser and was detected in the water trap equipped to its gas outlet channels (cf. to Fig. 1). Error bars and shaded areas indicate 95% confidence intervals calculated from at least three independent measurements, raw data that served the construction of the figure are accessible online [54].

the instantaneous increase of the cathodic potential shown in Fig. 3b, and by the (due to the nature of GC-based sampling, much slower) decrease of the measured FE_{CO} values. The trend of this shift is, however, distinctly different for the two GDEs, and while for the Nafion-bound catalyst layer a deterioration of electrolyser stability is imminent
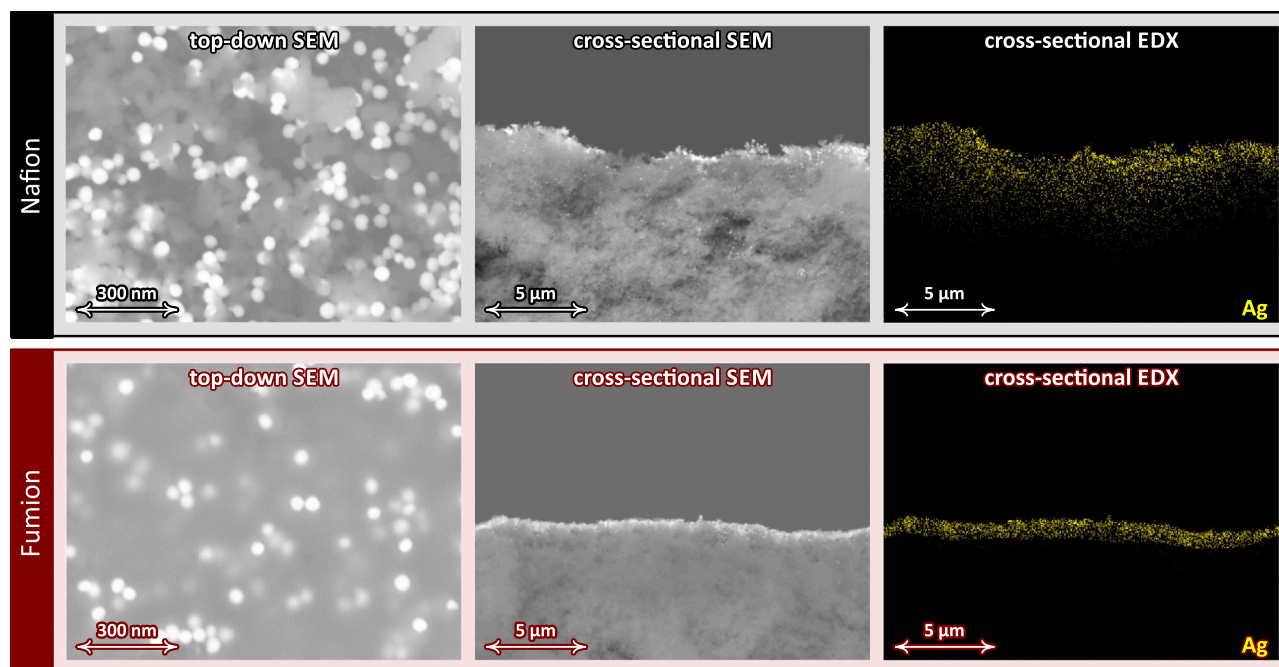
Fig. 2. SEM/EDX-based characterisation of Nafion-fixed (top row) and Fumion-fixed (bottom row) GDEs.

—already after the first 15 min of electrolysis, FE_{CO} drops to below 50%—, the Fumion-bound catalyst layer holds on for longer times, and even after 1 h long electrolysis, CO is still the majority product.

The reason of this difference in the electrolysis stability is not that electrolyte could not enter the Fumion-fixed GDE: as it can be seen in Fig. 3c, the amount of K^+ exiting through the outflow of the electrolyser is quite significant and the K^+ content of the trap keeps increasing steadily for the Fumion-containing GDE. The Nafion-fixed electrode, on the other hand, seems to allow no significant perspiration of K^+ ions through the electrolyser.

3.3. Fumion vs. Nafion: reasons behind different electrolysis lifespans unravelled by post mortem SEM–EDX investigations of GDEs

That the appearance of membrane-transported electrolytes have a key role in determining the stability of electrolyses is directly proven by the top-down and crosssectional SEM investigation of the two GDEs at different stages of electrolysis. The SEM micrographs in Fig. 4 were colourised based on the EDX-based elemental mapping of K and Ag to show the exact spots where precipitates and catalyst particles are located.

The as-prepared Nafion and Fumion-fixed electrodes look different in terms of apparent loading (top-down view) and the distribution of the catalyst particles (crosssectional view), due to reasons already described previously, in relation to Fig. 2. When the electrolysis starts, K^+-containing precipitates begin to appear (and their concentration evidently increases with the time of electrolysis) in both GDEs, however the spatial distribution and the accumulated amount of precipitates will be completely different for the two studied systems.

In Nafion-fixed GDEs, K^+ preferentially appears on-top of the catalyst layer, and plaques of precipitates tend to cover rather quickly the Ag NP catalyst particles. At the final stage of electrolysis, and this is well observable both in the top-down and cross-sectional SEM images, only some very little part of the catalyst layer remains active due to the formation of an about 3 μm thick $K_2CO_3/KHCO_3$ plaque formed over it. This is clearly the reason for which the Nafion-fixed GDE at this point already loses almost all its ability to reduce CO_2 to CO. The amount of K^+ that could enter —primarily at the beginning of electrolysis— the deeper layers of the MPL is significantly less than what is retained in the plaque. Note that after it is formed, the plaque should not only inhibit the electrolysis process, but should also hinder the further entry of K^+ ions into the MPL, which explains why the Nafion-fixed GDE allows almost no K^+ perspiration (Fig. 3c).

Fumion-fixed GDEs behave utterly differently compared to Nafion-fixed ones: not in the sense that in this case, clear signs of precipitate formations would not be visible (the amount of K^+, both on-top and within the GDL, clearly increases with the time of electrolysis, Fig. 4) but rather because the distribution of the precipitates is clearly more
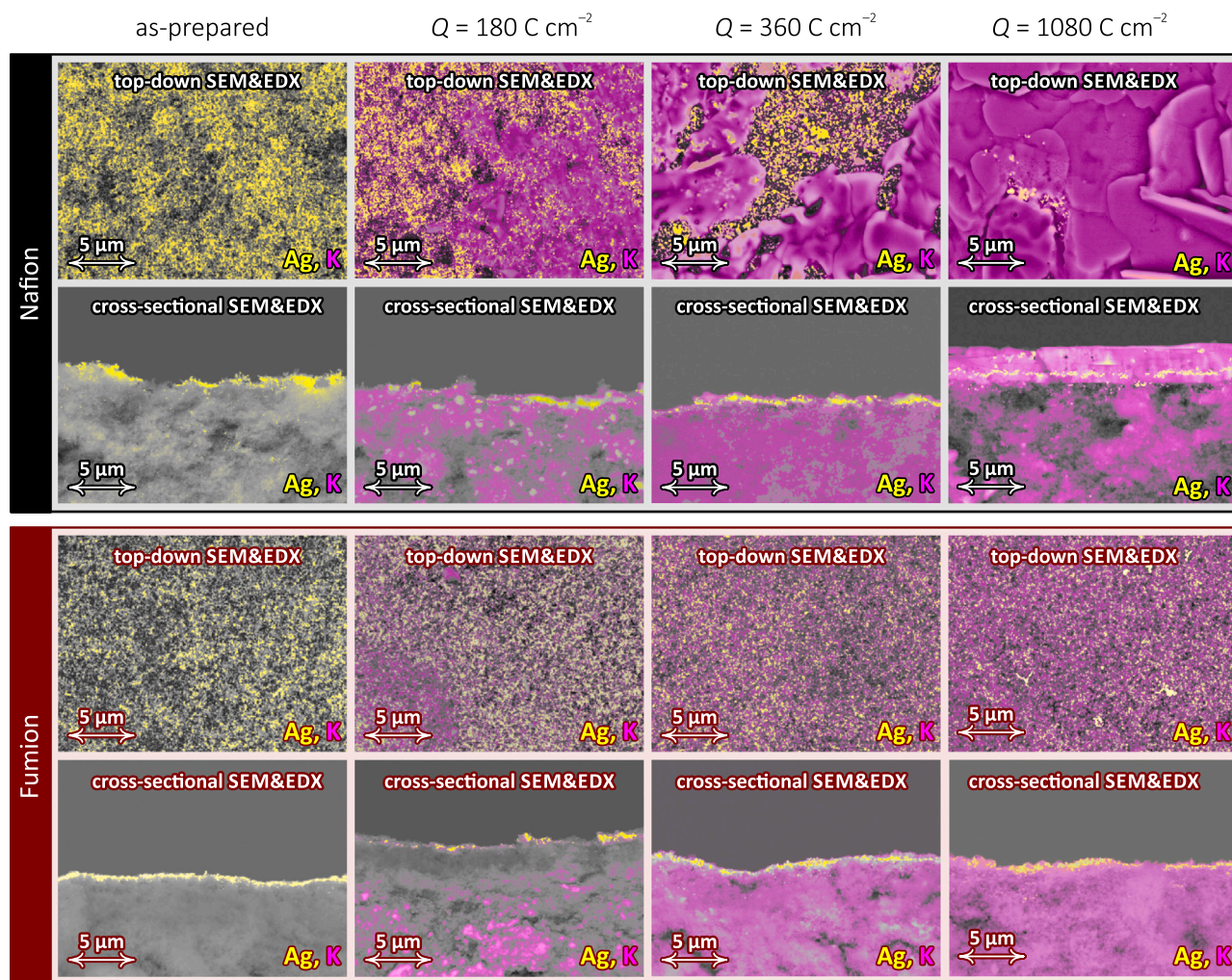

Fig. 4. Top-down and cross-sectional images recorded of Nafion and Fumion-fixed GDEs at different stages of electrolysis (after the passage of the indicated amount of charge). The images were colourised based on elemental EDX mapping: yellow colour stands for Ag, magenta for K-rich spots. The original SEM images and corresponding EDX maps are accessible online [54].

homogeneous in Fumion-fixed GDEs. Here, no distinct plaque formation is observed, and the formed precipitates seem to penetrate more uniformly the deeper regions of the MPLs. For the majority of the formed K⁺ salts it is still possible to perspire through the GDE structure, and eventually to exit the electrolyser—these salts can be detected in the water trap equipped to the gas outflow (Fig. 3c).

That the Fumion-fixed GDE retains its activity for a longer time than its Nafion-fixed alternative can clearly be explained by that the formed precipitates cover much less of the catalyst layer on-top of the Fumion-fixed GDE. Formed precipitates, on the other hand, do seem to penetrate the GDL structure to considerable extent, where they probably flood some portion of the micropores —this causes the about 50% drop of the Faradaic efficiency over the 1-hour electrolysis—, but this effect seems to be less detrimental than that of the plaque formation on-top of the catalyst layer, seen in the case of Nafion-fixed electrodes. It seems to be a plausible assumption that this improved performance of Fumion-fixed GDEs is due to the relatively compact, jelly film-like nature of Fumion that, as opposed to Nafion, does not penetrate and clogs the micropores of the MPL, however that is still somewhat permeable to K⁺ ions.

As the ultimate source of K⁺ ions in the studied electrolyser configuration is the anolyte, we carried out additional experiments utilising a 0.2 (instead of 2.0) mol dm⁻³ KOH solution as anolyte (see Figs. S4 and S5 in Supporting Information). It seemed, however, that also this decreased anolyte concentration is high enough to cause very similar stability issues and plaque formation during electrolysis on Nafion-bound GDEs.

In order to further support the hypothesis that Fumion-bound GDEs are superior to Nafion-bound electrodes due to that they enable more effective electrolyte perspiration, we had to rule out two alternative explanations; namely, that *i.)* the deficient stability of Nafion-bound GDEs could also be caused by the deeper penetration (and, as a result, partial deactivation) of the Ag NPs into the MPL, as was shown in Fig. 2; and *ii.)* that specific chemical interactions between the lipoic acid capping agent and the used ionomers may also be responsible for the observed durability differences of Fumion and Nafion-bound GDEs.

As to the first point, we found that in case we apply spray coating (instead of vacuum filtration) to cover the GDL with the catalyst ink, the aforementioned penetration of Ag NPs will occur to a considerably less extent (see Fig. S7 of Supporting Information), while the same difference between the stability of Nafion and Fumion fixed GDEs will remain to be observed (Fig. S8 of Supporting Information).

As to the second point, we also prepared GDEs using another two

capping agents —PVP and BPEI— with structures very different from that of lipoic acid, and we still observed (see Fig. S9 in Supporting Information) that Fumion-fixed GDEs retain their stability for longer times than Nafion-fixed ones, in a way that is rather similar for lipoic acid stabilised NPs.

The above experiments further support the conclusion of findings shown in Figs. 3 and 4: that is, efficient perspiration needs to be maintained in the zero-gap MEA to avoid plaque formation over the catalyst layer and resulting stability losses. From this point of view, Fumion-bound GDEs seem to perform better than their Nafion-fixed alternatives—however, upholding the efficiency of electrolysis is not the only advantage that Fumion offers.

3.4. The role of ionomers in protecting catalyst NPs from degradation

Another beneficial effect of the Fumion layer is that it protects most Ag NPs from degradation. If after 1 h electrolysis, we clean away (by water rinsing, see the Experimental Section) the formed precipitates from the top of the GDEs, we can use SEM-based analysis to detect the morphological changes of catalyst particles. Fig. 5 shows that in case of both electrodes, the initial size distribution of the NPs was almost monodisperse, centred around approximately 50 nm. During electrolysis, in case of the Nafion-bound electrode, severe degradation occurred, as a result of which many particles merged into large conglomerates, and the size distribution became flattened. A tendency towards the formation of large aggregates can also be noticed in the case of the Fumion-fixed GDE; however, in this case the protective Fumion layer seems to keep the big majority of the particles immobile, and as a result, the initial size distribution still remains dominant also after the electrolysis testing. We note here that following long-lasting electrolyses, the sharpness of the top-down SEM micrographs taken from Fumion-bound GDEs has apparently improved, and thus the number of exhibited NPs also seemed to increase (compare the SEM images of the "Fumion" panel in Fig. 5). This probably has to do with the degradation of the protective Fumion layer during electrolysis. That the large agglomerates formed to more extent on the Nafion-bound and to less on the Fumion-bound GDEs during electrolyses consist of Ag, is clearly proven by the EDX maps of Fig. S6 in Supporting Information.

3.5. Testing Fumion-bound GDEs with anolytes of different compositions

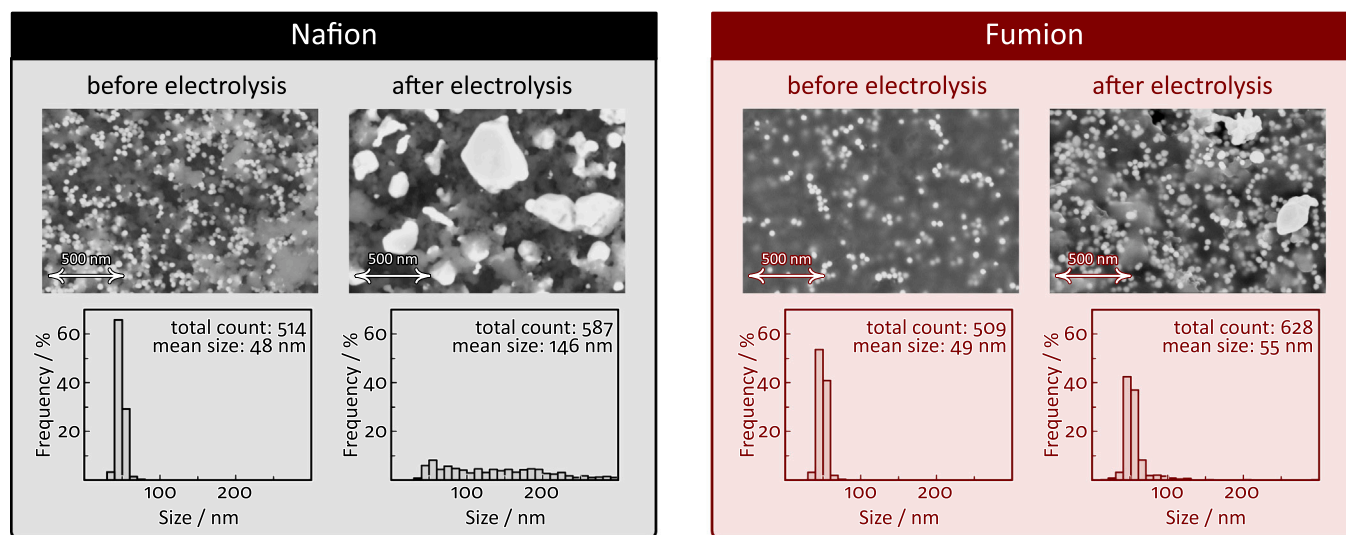The experiments described above all indicate that it is the relatively

Fig. 5. Top-down and cross-sectional images recorded of Nafion and Fumion-fixed GDEs at different stages of electrolysis (after the passage of the indicated amount of charge). The images were colourised based on elemental EDX mapping: yellow colour stands for Ag, magenta for K-rich spots. The original SEM images and corresponding EDX maps are accessible online [54].

good permeability of the Fumion layer to K$^+$ ions that enables a more long-lasting cell stability (compared to what can be achieved by using Nafion-bound GDEs), and that the ability of Fumion in upholding electrolyte perspiration is essential for the stable operation of CO$_2$ electrolysing zero-gap MEAs.

In order to further test the validity of this statement and to define its boundaries, we performed a set of further experiments in which Fumion-fixed GDEs (MEAs) were used in combination with anolytes of different compositions. Apart from KOH, LiOH, NaOH and CsOH solutions of 2 mol dm^{-3} concentration were used as anolyte in these experiments. As shown in Fig. 6, we found during electrolysis at a constant current density of 150 mA cm^{-2} that in case of a CsOH anolyte, the stability of electrolysis could slightly be improved (compared to when a KOH anolyte was applied). In case of NaOH, the durability of the electrolysis has already significantly decreased, and HER became prevailing over *ec*–CO$_2$RR already after 2 h of electrolysis. Furthermore, if NaOH was used as an electrolyte, results (see Fig. 6) also indicated the production formate ions at large scale (something that was not seen either in case of KOH or of CsOH). In the case when LiOH was used as an anolyte, the electrolysis broke down almost immediately —so that no product distribution could be determined— and the measured potential reached a saturation value, indicating that the control circuit cannot provide sufficient current for the electrolysis.

Also in these experiments we found that stability losses during electrolysis usually occur as a result of plaque (precipitate) formation over the GDE surfaces (Fig. 7), and that the time at which the electrolysis breaks down is mostly determined by two factors: the transport properties (the mobility) of the cations and the solubility of their carbonate salts. The SEM/EDX characterisation of GDEs at different stages of the electrolysis show that in case of K$^+$ and Cs$^+$, precipitates appear rather late over the catalyst layer, while the formation of Na$^+$ and, in particular, Li$^+$ carbonates on top of GDEs commences much earlier. This has to do with the greater (hydrodynamic) radius and the resulting reduced mobility of hydrated Na$^+$ and Li$^+$ ions, as well as with the limited

solubility of their carbonate salts (see Table 1 for data). A correlation between the diffusion coefficients of the cations and the solubility of their carbonate salts, as well as the stability time of electrolyses when different alkali hydroxides are used as anolytes are shown in Fig. 8. (The time of electrolysis stability we define here as the electrolysis time required for FE$_{H_2}$ to grow higher than 50%.).

The above experiments demonstrate that while the application of Fumion as an ionomer of catalyst inks usually leads to more prolonged electrolyser stabilities compared to when, e.g., a Nafion binder is used, precipitation inside Fumion-bound GDEs can still be observed, and this is what at the end determines the stability of the process. Apart from choosing the right ionomer material for the fabrication of GDEs, also the composition of the anolyte has thus to be taken into account in order to establish proper electrolyte management within CO reducing GDE-based MEAs, in alignment with novel findings of Garg et al. [56] and of Burdyny et al. [57].

4. Conclusion

In this paper we prepared Ag NPs containing catalyst inks by the application of two different binders: Nafion and Fumion. By using these inks, we created GDEs that we subjected, in a zero-gap MEA configuration, to *ec*–CO$_2$RR experiments. Although based on their wettabilities (Nafion-fixed GDEs are more hydrophobic than Fumion-fixed ones) we expected the opposite [48,49], we found that on Fumion-containing GDEs the selectivity of CO$_2$-to-CO conversion can be upheld for longer times.

By a post-electrolysis EDX-based elemental (K) analysis of precipitation patterns inside and on-top of the GDEs, combined with a mass spectrometric monitoring of the perspired electrolyte amount, we concluded that the poor performance of Nafion-fixed GDEs is due to the formation of K$_2$CO$_3$/KHCO$_3$ precipitate plaques over the catalyst layer that breaks down its activity in *ec*–CO$_2$RR. On Fumion-fixed GDEs this plaque formation was avoided, and while a protective ionomer layer
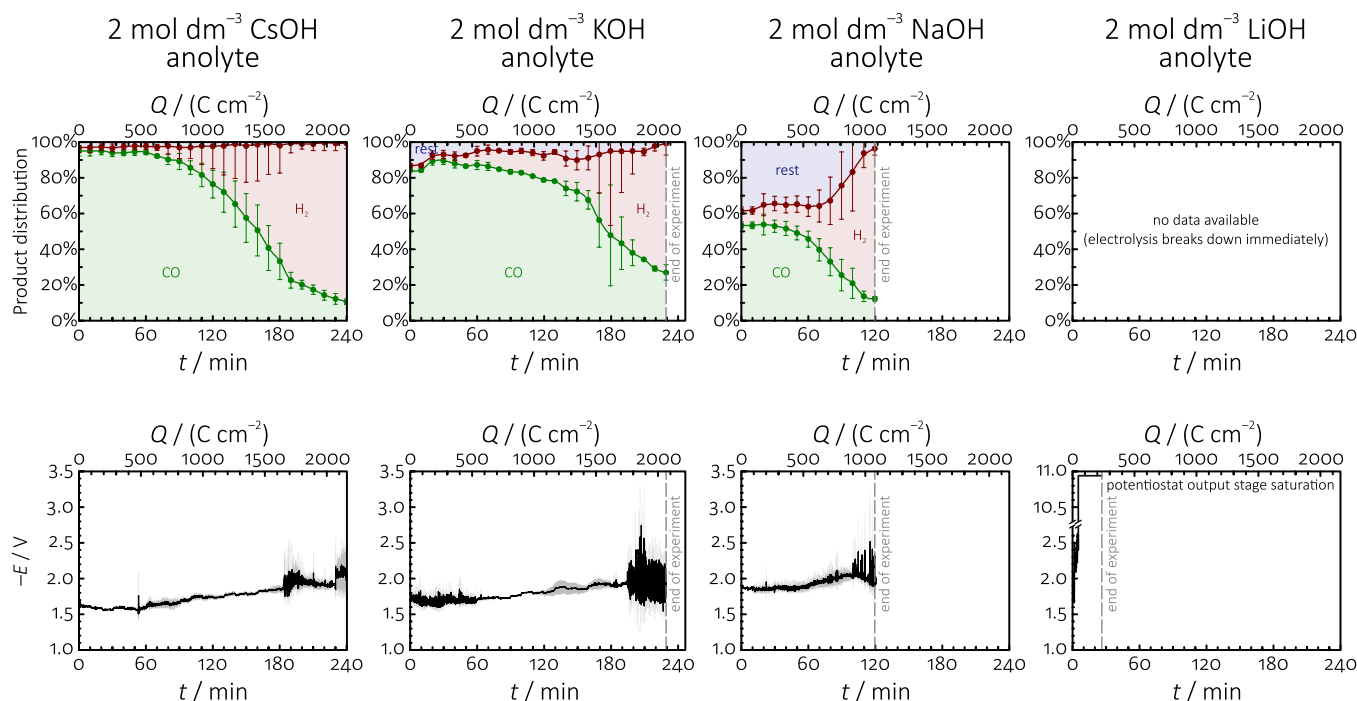

Fig. 6. Fumion-fixed GDEs are tested in *ec*–CO$_2$RR experiments in the cell shown in Fig. 1, using different anolyte compositions. The top row shows the time (charge) dependence of the product distribution, the bottom row the time (charge) dependence of the measured cathode potential. Applied current density: 150 mA cm^{-2}. Regions marked as "rest" in the product distribution plots probably correspond to the production of formate. (Slight amounts of formate were detected in the anode compartment of the electrolyser following the experiments: the amount of formate can however not be exactly quantified in the used set-up, due to its possible oxidation at the anode.)
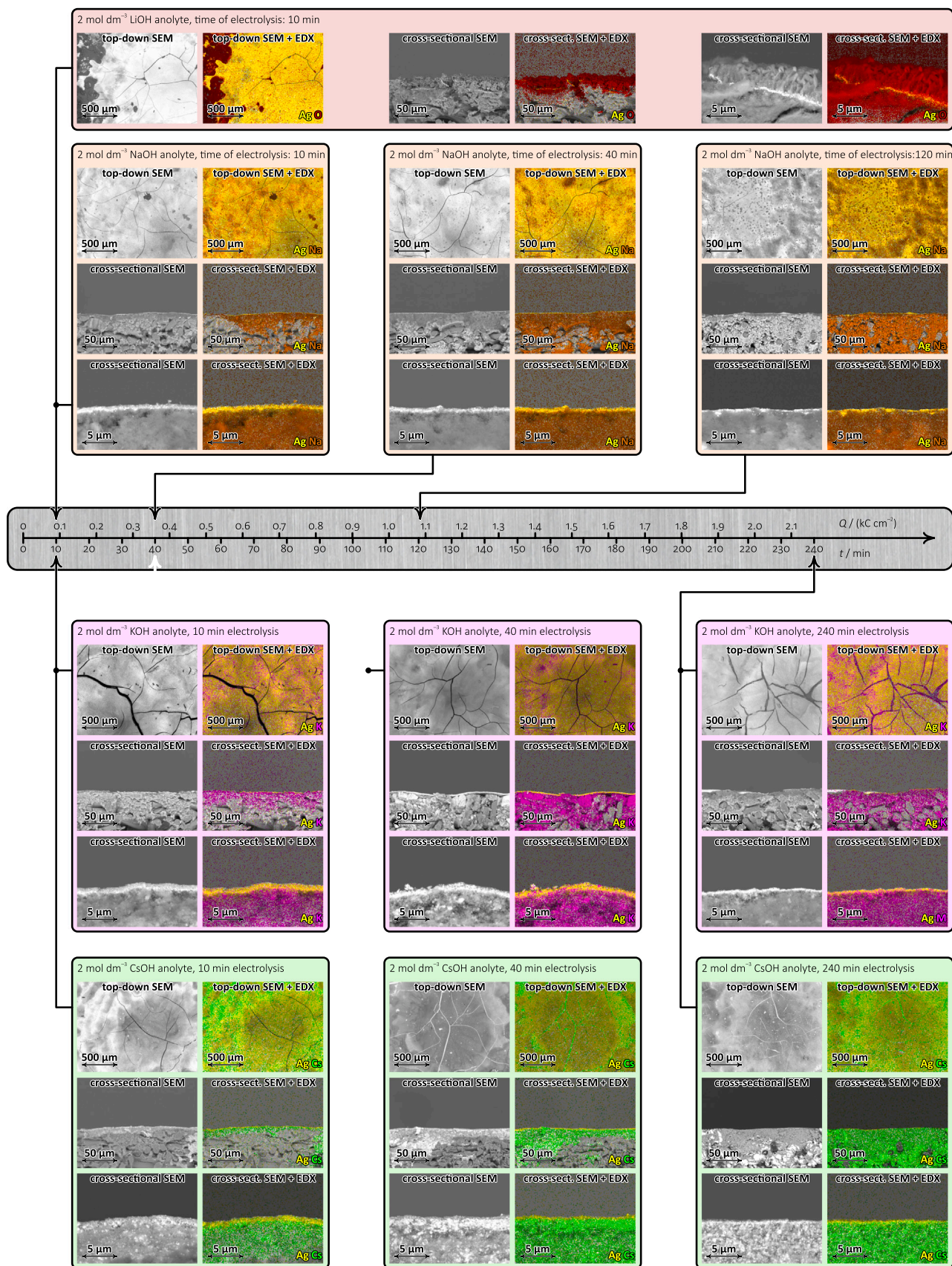
Fig. 7. Top-down and cross-sectional SEM and EDX investigation of Fumion-fixed GDEs following *ec*–CO$_2$RR stressing after electrolysis lasting different times (corresponding to different passed charge densities). LiOH, NaOH, KOH and CsOH were used as anolytes of the electrolyser. Elemental EDX mapping shows the formation of growing amounts of precipitates inside and on-top of the GDE structure as a function of increasing charge. For visualising Li$^+$ carbonate precipitates, elemental O mapping was applied. Applied current density: 150 mA cm^{-2}. Cf. to Fig. 6 for electrochemical measurement data.

Table 1

Physico-chemical parameters (Λ_0: molar conductivity at infinite dilution, D_0: diffusion coefficient at infinite dilution, r_{Stokes}: hydrodynamic radius) of the different hydrated alkali cations studied in this paper, as well as the solubility of their carbonate salt ($b_{max,\,M_2CO_3}$) expressed in molality and the approximate stability time (t_{stab}) of electrolyses when the given alkali hydroxide is used as anolyte of the electrolyser. Data are taken from Ref. [55]; transport parameters correspond to 25 °C, solubilities to 15 °C temperature.

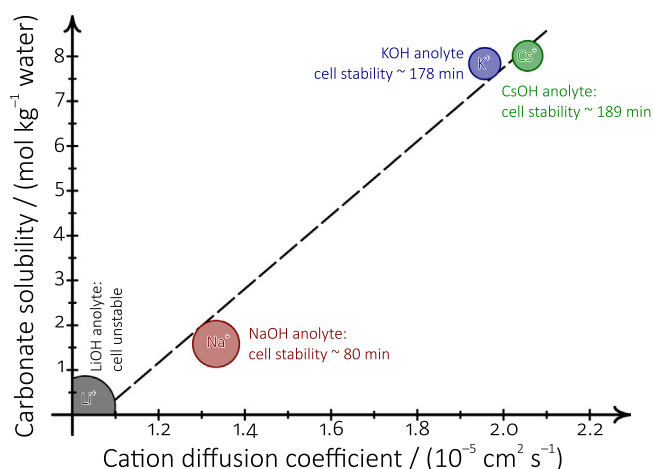|	Li$^+$	Na$^+$	K$^+$	Cs$^+$
Λ_0 / (S cm^2 mol^{-1})	38.66	50.08	73.48	77.20
D_0 / (10^{-5} cm^2 s^{-1})	1.029	1.333	1.957	2.056
r_{Stokes} / Å	2.386	1.842	1.255	1.195
$b_{max,\,M_2CO_3}$ / (mol kg^{-1})	0.1894	1.581	7.839	8.011
t_{stab} / s	~5	~80	~178	~189

Fig. 8. Plot showing a direct correlation between the diffusion coefficients (scaled mobilities) of the studied cations and the solubilities of their carbonate salts, as well as the stability of electrolyser cells operated with the corresponding 2 mol dm^{-3} hydroxide solutions. See Table 1 for numerical data.

kept most of the Ag NP catalyst particles active, a majority amount of the K$^+$-containing electrolyte that penetrated through the membrane could perspire through the GDE and exit the electrolyser through the gas outflow line.

Our results indicate that from the point of view of upholding the stability of CO$_2$ electrolyses in zero-gap MEA-based cathode configurations, the importance of good electrolyte management (effective perspiration) is even higher than that of the wettability properties of GDEs [48–51].

By carrying out experiments with Fumion-fixed GDEs in combination with anolytes of different compositions (KOH, CsOH, NaOH and LiOH), we demonstrated that stable electrolysis (efficient perspiration) can more be upheld in the order Cs$^+$ > K$^+$ > Na$^+$ >> Li$^+$; that is, in case when smaller (more mobile) cations are used, the carbonates of which exhibit greater solubility in water.

CRediT authorship contribution statement

Menglong Liu: Investigation, Experiments, Data curation, Writing – first draft. **Ying Kong:** Investigation, Experiments. **Huifang Hu:** Investigation, Experiments. **Iván Zelocualtecatl Montiel:** Investigation, Experiments. **Viliam Kolivoška:** Conceptualization, Methodology. **Alexander V. Rudnev:** Conceptualization, Methodology. **Yuhui Hou:** Conceptualization, Methodology. **Rolf Erni:** TEM measurements. **Soma Vesztergom:** Conceptualization, Methodology, Visualization, Data analysis, Writing, Funding acquisition. **Peter Broekmann:**

Conceptualization, Methodology, Writing – review & editing, Supervision, Funding acquisition.

Declaration of Competing Interest

The authors declare the following financial interests/personal relationships which may be considered as potential competing interests: Peter Broekmann reports financial support was provided by National Center of Competence in Research Catalysis. Soma Vesztergom reports financial support was provided by National Research Development and Innovation Office. Viliam Kolivoska reports financial support was provided by Czech Science Foundation.

Data availability

The Zenodo service will be used for the publication of ALL relevant research data. Using the doi shown in Ref. 54 of the paper, all research data will be made accessible upon publication of the paper.

Appendix A. Supplementary material

Supplementary data associated with this article can be found in the online version at doi:10.1016/j.apcatb.2023.122885.

References

[1] X. Tan, C. Yu, Y. Ren, S. Cui, W. Li, J. Qiu, Recent advances in innovative strategies for the CO$_2$ electroreduction reaction, Energy Environ. Sci. 14 (2021) 765–780, https://doi.org/10.1039/d0ee02981e.

[2] G. Centi, S. Perathoner, Z.S. Rak, Reduction of greenhouse gas emissions by catalytic processes, Appl. Catal. B 41 (2003) 143–155, https://doi.org/10.1016/s0926-3373(02)00207-2.

[3] Z.W. Seh, J. Kibsgaard, C.F. Dickens, I. Chorkendorff, J.K. Nørskov, T.F. Jaramillo, Combining theory and experiment in electrocatalysis: insights into materials design, Science 355 (2017) eaad4998, https://doi.org/10.1126/science.aad4998.

[4] S. Ma, M. Sadakiyo, M. Heima, R. Luo, R.T. Haasch, J.I. Gold, M. Yamauchi, P.J. A. Kenis, Electroreduction of carbon dioxide to hydrocarbons using bimetallic Cu–Pd catalysts with different mixing patterns, J. Am. Chem. Soc. 139 (2017) 47–50, https://doi.org/10.1021/jacs.6b10740.

[5] T. Jaster, A. Gawel, D. Siegmund, J. Holzmann, H. Lohmann, E. Klemm, U.-P. Apfel, Electrochemical CO$_2$ reduction toward multicarbon alcohols — the microscopic world of catalysts & process conditions, iScience 25 (2022), 104010, https://doi.org/10.1016/j.isci.2022.104010.

[6] J. Albo, A. Sáez, J. Solla-Gullón, V. Montiel, A. Irabien, Production of methanol from CO$_2$ electroreduction at Cu$_2$O and Cu$_2$O/ZnObased electrodes in aqueous solution, Appl. Catal. B 176–177 (2015) 709–717, https://doi.org/10.1016/j.apcatb.2015.04.055.

[7] Y. Zheng, A. Vasileff, X. Zhou, Y. Jiao, M. Jaroniec, S.-Z. Qiao, Understanding the roadmap for electrochemical reduction of CO$_2$ to multi-carbon oxygenates and hydrocarbons on copper-based catalysts, J. Am. Chem. Soc. 141 (2019) 7646–7659, https://doi.org/10.1021/jacs.9b02124.

[8] X. Su, Y. Sun, L. Jin, L. Zhang, Y. Yang, P. Kerns, B. Liu, S. Li, J. He, Hierarchically porous Cu/Zn bimetallic catalysts for highly selective CO$_2$ electroreduction to liquid C$_2$ products, Appl. Catal. B 269 (2020) 118800, https://doi.org/10.1016/j.apcatb.2020.118800.

[9] C.-T. Dinh, F.P.G. de Arquer, D. Sinton, E.H. Sargent, High rate, selective, and stable electroreduction of CO$_2$ to CO in basic and neutral media, ACS Energy Lett. 3 (2018) 2835–2840, https://doi.org/10.1021/acsenergylett.8b01734.

[10] T. Haas, R. Krause, R. Weber, M. Demler, G. Schmid, Technical photosynthesis involving CO$_2$ electrolysis and fermentation, Nat. Catal. 1 (2018) 32–39, https://doi.org/10.1038/s41929-017-0005-1.

[11] Y. Hori, Electrochemical CO$_2$ reduction on metal electrodes, in: C.G. Vayenas, R. E. White, M.E. Gamboa-Aldeco (Eds.), Modern Aspects of Electrochemistry Vol. 42, Springer, New York, 2008, pp. 89–189, https://doi.org/10.1007/978-0-387-49489-0.

[12] S.A. Mahyoub, F.A. Qaraah, C. Chen, F. Zhang, S. Yan, Z. Cheng, An overview on the recent developments of Ag-based electrodes in the electrochemical reduction of CO$_2$ to CO, Sustain. Energy Fuels 4 (2020) 50–67, https://doi.org/10.1039/c9se00594c.

[13] D. Sun, X. Xu, Y. Qin, S.P. Jiang, Z. Shao, Rational design of Ag based catalysts for the electrochemical CO$_2$ reduction to CO: A review, ChemSusChem 13 (2019) 39–58, https://doi.org/10.1002/cssc.201902061.

[14] Y. Li, C. Chen, R. Cao, Z. Pan, H. He, K. Zhou, Dual-atom Ag$_2$/graphene catalyst for efficient electroreduction of CO$_2$ to CO, Appl. Catal. B 268 (2020), 118747, https://doi.org/10.1016/j.apcatb.2020.118747.

[15] H. Hu, M. Liu, Y. Kong, V. Kolivoška, A. Rudnev, Y. Hou, R. Erni, S. Vesztergom, P. Broekmann, Effective perspiration is essential to uphold the stability of zero-gap MEA-based CO$_2$ electrolysers, J. Mater. Chem. A 11 (2023) 5083–5094, https://doi.org/10.1039/D2TA06965B.

[16] Z. Yang, D. Li, L. Xing, H. Xiang, J. Xuan, S. Cheng, E.H. Yu, A. Yang, Modeling and upscaling analysis of gas diffusion electrode-based electrochemical carbon dioxide reduction systems, ACS Sustain. Chem. Eng. 9 (2020) 351–361, https://doi.org/10.1021/acssuschemeng.0c07387.

[17] A. Gawel, T. Jaster, D. Siegmund, J. Holzmann, H. Lohmann, E. Klemm, U.-P. Apfel, Electrochemical CO$_2$ reduction – the macroscopic world of electrode design, reactor concepts & economic aspects, iScience 25 (2022), 104011, https://doi.org/10.1016/j.isci.2022.104011.

[18] D.M. Weekes, D.A. Salvatore, A. Reyes, A. Huang, C.P. Berlinguette, Electrolytic CO$_2$ reduction in a flow cell, Acc. Chem. Res. 51 (2018) 910–918, https://doi.org/10.1021/acs.accounts.8b00010.

[19] D. Higgins, C. Hahn, C. Xiang, T.F. Jaramillo, A.Z. Weber, Gas-diffusion electrodes for carbon dioxide reduction: a new paradigm, ACS Energy Lett. 4 (2019) 317–324, https://doi.org/10.1021/acsenergylett.8b02035.

[20] T. Burdyny, W.A. Smith, CO$_2$ reduction on gas-diffusion electrodes and why catalytic performance must be assessed at commercially relevant conditions, Energy Environ. Sci. 12 (2019) 1442–1453, https://doi.org/10.1039/c8ee03134g.

[21] N.T. Nesbitt, T. Burdyny, H. Simonson, D. Salvatore, D. Bohra, R. Kas, W.A. Smith, Liquid–solid boundaries dominate activity of CO$_2$ reduction on gas-diffusion electrodes, ACS Catal. 10 (2020) 14093–14106, https://doi.org/10.1021/acscatal.0c03319.

[22] U.O. Nwabara, M.P. de Heer, E.R. Cofell, S. Verma, E. Negro, P.J.A. Kenis, Towards accelerated durability testing protocols for CO$_2$ electrolysis, J. Mater. Chem. A 8 (2020) 22557–22571, https://doi.org/10.1039/d0ta08695a.

[23] E.W. Lees, B.A.W. Mowbray, F.G.L. Parlane, C.P. Berlinguette, Gas diffusion electrodes and membranes for CO$_2$ reduction electrolysers, Nat. Rev. Mater. 7 (2021) 55–64, https://doi.org/10.1038/s41578-021-00356-2.

[24] Y. Luo, K. Zhang, Y. Li, Y. Wang, Valorizing carbon dioxide via electrochemical reduction on gas-diffusion electrodes, InfoMat 3 (2021) 1313–1332, https://doi.org/10.1002/inf2.12253.

[25] W. Liu, S. Wei, P. Bai, C. Yang, L. Xu, Robust coal matrix intensifies electron/substrate interaction of nickel-nitrogen (Ni-N) active sites for efficient CO$_2$ electroreduction at industrial current density, Appl. Catal. B 299 (2021), 120661, https://doi.org/10.1016/j.apcatb.2021.120661.

[26] H. Rabiee, L. Ge, X. Zhang, S. Hu, M. Li, S. Smart, Z. Zhu, H. Wang, Z. Yuan, Stand-alone asymmetric hollow fiber gas-diffusion electrodes with distinguished bronze phases for high-efficiency CO$_2$ electrochemical reduction, Appl. Catal. B 298 (2021), 120538, https://doi.org/10.1016/j.apcatb.2021.120538.

[27] H. Rabiee, L. Ge, J. Zhao, X. Zhang, M. Li, S. Hu, S. Smart, T.E. Rufford, Z. Zhu, H. Wang, Z. Yuan, Regulating the reaction zone of electrochemical CO$_2$ reduction on gas-diffusion electrodes by istinctive hydrophilic-hydrophobic catalyst layers, Appl. Catal. B 310 (2022), 121362, https://doi.org/10.1016/j.apcatb.2022.121362.

[28] D. Giusi, M. Miceli, C. Genovese, G. Centi, S. Perathoner, C. Ampelli, In situ electrochemical characterization of Cu$_x$O-based gasdiffusion electrodes (GDEs) for CO$_2$ electrocatalytic reduction in presence and absence of liquid electrolyte and relationship with c2+ products formation, Appl. Catal. B 318 (2022), 121845, https://doi.org/10.1016/j.apcatb.2022.121845.

[29] K. Yang, R. Kas, W.A. Smith, T. Burdyny, Role of the carbon-based gas diffusion layer on flooding in a gas diffusion electrode cell for electrochemical CO$_2$ reduction, ACS Energy Lett. 6 (2020) 33–40, https://doi.org/10.1021/acsenergylett.0c02184.

[30] S. Alinejad, J. Quinson, G.K.H. Wiberg, N. Schlegel, D. Zhang, Y. Li, S. Reichenberger, S. Barcikowski, M. Arenz, Electrochemical reduction of CO$_2$ on Au electrocatalysts in a zero-gap, half-cell gas diffusion electrode setup: a systematic performance evaluation and comparison to an H-cell setup, ChemElectroChem 9 (12) (2022), e202200341, https://doi.org/10.1002/celc.202200341.

[31] M. de, J. Gálvez-Vázquez, P. Moreno-García, H. Xu, Y. Hou, H. Hu, I.Z. Montiel, A. V. Rudnev, S. Alinejad, V. Grozovski, B.J. Wiley, M. Arenz, P. Broekmann, Environment matters: CO$_2$ electrocatalyst performance testing in a gas-fed zero-gap electrolyzer, ACS Catal. 10 (2020) 13096–13108, https://doi.org/10.1021/acscatal.0c03609.

[32] D.A. Salvatore, C.M. Gabardo, A. Reyes, C.P. O'Brien, S. Holdcroft, P. Pintauro, B. Bahar, M. Hickner, C. Bae, D. Sinton, E.H. Sargent, C.P. Berlinguette, Designing

[33] A. Reyes, R.P. Jansonius, B.A.W. Mowbray, Y. Cao, D.G. Wheeler, J. Chau, D. J. Dvorak, C.P. Berlinguette, Managing hydration at the cathode enables efficient CO$_2$ electrolysis at commercially relevant current densities, ACS Energy Lett. 5 (2020) 1612–1618, https://doi.org/10.1021/acsenergylett.0c00637.

[34] M.E. Leonard, L.E. Clarke, A. Forner-Cuenca, S.M. Brown, F.R. Brushett, Investigating electrode flooding in a flowing electrolyte, gas-fed carbon dioxide electrolyzer, ChemSusChem 13 (2020) 400–411, https://doi.org/10.1002/cssc.201902547.

[35] B. Kim, F. Hillman, M. Ariyoshi, S. Fujikawa, P.J.A. Kenis, Effects of composition of the micro porous layer and the substrate on performance in the electrochemical reduction of CO$_2$ to CO, J. Power Sources 312 (2016) 192–198, https://doi.org/10.1016/j.jpowsour.2016.02.043.

[36] G.O. Larrazábal, P. Strøm-Hansen, J.P. Heli, K. Zeiter, K.T. Therkildsen, I. Chorkendorff, B. Seger, Analysis of mass flows and membrane cross-over in CO$_2$ reduction at high current densities in an MEA-type electrolyzer, ACS Appl. Mater. Interfaces 11 (44) (2019) 41281–41288, https://doi.org/10.1021/acsami.9b13081.

[37] B. Endrődi, E. Kecsenovity, A. Samu, F. Darvas, R.V. Jones, V. Török, A. Danyi, C. Janáky, Multilayer electrolyzer stack converts carbon dioxide to gas products at high pressure with high efficiency, ACS Energy Lett. 4 (2019) 1770–1777, https://doi.org/10.1021/acsenergylett.9b01142.

[38] W.H. Lee, Y.-J. Ko, Y. Choi, S.Y. Lee, C.H. Choi, Y.J. Hwang, B.K. Min, P. Strasser, H.-S. Oh, Highly selective and scalable CO$_2$ to CO electrolysis using coral-nanostructured Ag catalysts in zero-gap configuration, Nano Energy 76 (2020), 105030, https://doi.org/10.1016/j.nanoen.2020.105030.

[39] A.A. Samu, A. Kormányos, E. Kecsenovity, N. Szilágyi, B. Endrődi, C. Janáky, Intermittent operation of CO$_2$ electrolyzers at industrially relevant current densities, ACS Energy Lett. 7 (2022) 1859–1861, https://doi.org/10.1021/acsenergylett.2c00923.

[40] M. Liu, Y. Kong, H. Hu, N. Kovács, C. Sun, I. Zelocualtecatl Montiel, M. de, J. Gálvez Vázquez, Y. Hou, M. Mirolo, I. Martens, J. Drnec, S. Vesztergom, P. Broekmann, The capping agent is the key: Structural alterations of ag NPs during CO$_2$ electrolysis probed in a zero-gap gas-flow configuration, J. Catal. 404 (2021) 371–382, https://doi.org/10.1016/j.jcat.2021.10.016.

[41] Y. Kong, H. Hu, M. Liu, Y. Hou, V. Kolivoška, S. Vesztergom, P. Broekmann, Visualisation and quantification of flooding phenomena in gas diffusion electrodes used for electrochemical CO$_2$ reduction: a combined EDX/ICP–MS approach, J. Catal. 408 (2022) 1–8, https://doi.org/10.1016/j.jcat.2022.02.014.

[42] Y. Kong, M. Liu, H. Hu, Y. Hou, S. Vesztergom, M. de, J. Gálvez Vázquez, I. Zelocualtecatl Montiel, V. Kolivoška, P. Broekmann, Cracks as efficient tools to mitigate flooding in gas diffusion electrodes used for the electrochemical reduction of carbon dioxide, Small Methods (2022), 2200369, https://doi.org/10.1002/smtd.202200369.

[43] P. Jeanty, C. Scherer, E. Magori, K. Wiesner-Fleischer, O. Hinrichsen, M. Fleischer, Upscaling and continuous operation of electrochemical CO$_2$ to CO conversion in aqueous solutions on silver gas diffusion electrodes, J. CO$_2$ Util. 24 (2018) 454–462, https://doi.org/10.1016/j.jcou.2018.01.011.

[44] B. De Mot, J. Hereijgers, M. Duarte, T. Breugelmans, Influence of flow and pressure distribution inside a gas diffusion electrode on the performance of a flow-by CO$_2$ electrolyzer, Chem. Eng. J. 378 (2019), 122224, https://doi.org/10.1016/j.cej.2019.122224.

[45] B. De Mot, M. Ramdin, J. Hereijgers, T.J.H. Vlugt, T. Breugelmans, Direct water injection in catholyte-free zero-gap carbon dioxide electrolyzers, ChemElectroChem 7 (2020) 3839–3843, https://doi.org/10.1002/celc.202000961.

[46] U.O. Nwabara, E.R. Cofell, S. Verma, E. Negro, P.J.A. Kenis, Durable cathodes and electrolyzers for the efficient aqueous electrochemical reduction of CO$_2$, ChemSusChem 13 (2020) 855–875, https://doi.org/10.1002/cssc.201902933.

[47] A. Pătru, T. Binninger, B. Pribyl, T.J. Schmidt, Design principles of bipolar electrochemical co-electrolysis cells for efficient reduction of carbon dioxide from gas phase at low temperature, J. Electrochem. Soc. 166 (2019) F34–F43, https://doi.org/10.1149/2.1221816jes.

[48] U.O. Nwabara, A.D. Hernandez, D.A. Henckel, X. Chen, E.R. Cofell, M.P. de Heer, S. Verma, A.A. Gewirth, P.J.A. Kenis, Binderfocused approaches to improve the stability of cathodes for CO$_2$ electroreduction, ACS Appl. Energy Mater. 4 (2021) 5175–5186, https://doi.org/10.1021/acsaem.1c00715.

[49] M. Li, M.N. Idros, Y. Wu, T. Burdyny, S. Garg, X.S. Zhao, G. Wang, T.E. Rufford, The role of electrode wettability in electrochemical reduction of carbon dioxide, J. Mater. Chem. A 9 (2021) 19369–19409, https://doi.org/10.1039/d1ta03636j.

[50] Z. Xing, L. Hu, D.S. Ripatti, X. Hu, X. Feng, Enhancing carbon dioxide gas-diffusion electrolysis by creating a hydrophobic catalyst microenvironment, Nat. Commun. 12 (2021) 136, https://doi.org/10.1038/s41467-020-20397-5.

[51] K.U. Hansen, F. Jiao, Hydrophobicity of CO$_2$ gas diffusion electrodes, Joule 5 (2021) 754–757, https://doi.org/10.1016/j.joule.2021.02.005.

[52] Z. Liu, H. Yang, R. Kutz, R.I. Masel, CO$_2$ electrolysis to CO and O$_2$ at high selectivity, stability and efficiency using Sustainion membranes, J. Electrochem. Soc. 165 (2018) J3371, https://doi.org/10.1149/2.0501815jes.

[53] A.V. Rudnev, Online chromatographic detection, in: K. Wandelt (Ed.), Encyclopedia of Interfacial Chemistry, Elsevier, Amsterdam, 2018, pp. 321–325, https://doi.org/10.1016/b978-0-12-409547-2.13564-4.

[54] M. Liu, H. Hu, Y. Kong, I. Zelocualtecatl Montiel, V. Kolivoška, A.V. Rudnev, Y. Hou, S. Vesztergom, P. Broekmann, Raw data for the article "The role of ionomers in the electrolyte management of zero-gap MEA-based CO2 electrolysers: A Fumion vs. Nafion comparison", Zenodo. ⟨https://doi.org/10.5281/zenodo.7117080⟩.

[55] W.M. Haynes. CRC Handbook of Chemistry and Physics, 97th ed., CRC Press, Boca Raton FL, 2017. Section 5.

[56] S. Garg, Q. Xu, A.B. Mossa, M. Mirolo, W. Denga, I. Chorkendorff, J. Drnec, B. Seger, How alkali cations affect salt precipitation and CO2 electrolysis performance in membrane electrode assembly electrolyzers Energy, Environ. Sci. 16 (2023) 1631–1643, https://doi.org/10.1039/D2EE03725D.

[57] M. Sassenburg, M. Kelly, S. Subramanian, W.A. Smith, T. Burdyny, Zero-gap electrochemical CO$_2$ reduction cells: challenges and operational strategies for prevention of salt precipitation, ACS Energy Lett. 8 (2023) 321–331, https://doi.org/10.1021/acsenergylett.2c01885.